International Journal of Heat and Mass Transfer 70 (2014) 954–964

Contents lists available at ScienceDirect

International Journal of Heat and Mass Transfer

journal homepage: www.elsevier.com/locate/ijhmt

Molecular dynamics simulations of thermal conductivity of carbon nanotubes: Resolving the effects of computational parameters

Richard N. Salaway [a], Leonid V. Zhigilei [b,*]

[a] Department of Mechanical & Aerospace Engineering, University of Virginia, 122 Engineer's Way, Charlottesville, VA 22904-4746, USA
[b] Department of Materials Science & Engineering, University of Virginia, 395 McCormick Road, Charlottesville, VA 22904-4745, USA

ARTICLE INFO

Article history:
Received 10 September 2013
Received in revised form 21 November 2013
Accepted 21 November 2013

Keywords:
Thermal conductivity
Carbon nanotube
Molecular dynamics simulations

ABSTRACT

Predicting thermal conductivity, k, of carbon nanotubes (CNTs) has been the focus of many molecular dynamics (MD) simulation studies reported in the literature. The values of k obtained in these studies exhibit a large, up to an order of magnitude, variability that is commonly attributed to the variations in the computational setups adopted in different studies. The sensitivity of the computational results to the choice of individual parameters of the simulation setups, however, has not been systematically investigated and is often overlooked when the predicted values of k are compared across the literature. Here we present the results of several series of simulations specifically designed to evaluate the effects of common computational parameters of non-equilibrium MD (NEMD), such as the type of boundary conditions, size and location of heat bath regions, definition of the CNT length, and the choice of interatomic potential, on the computational predictions. The length dependence of thermal conductivity is found to exhibit a gradual transition from a strong increase of k with CNT length for nanotubes that are shorter than ~200 nm to a much weaker dependence for longer CNTs, reflecting the transition from ballistic to diffusive-ballistic heat transport regimes. The effect of increasing length of thermal bath regions is found to be nearly indistinguishable from the effect of increasing length of the unperturbed region between the bath regions, suggesting that the value of k is defined by the total length of the CNT (including the length of the heat bath regions) in NEMD simulations employing uni-directional heat flux. The choice of interatomic potential is shown to be responsible for an up to fourfold variability in predictions of k for otherwise identical simulation conditions. Overall, the results of this study help elucidate the cause of quantitative discrepancies across published data and provide recommendations on the choice of simulation setups that may improve the consistency of the computational predictions.

1. Introduction

The exceptionally high thermal conductivity of carbon nanotubes (CNTs) revealed in experiments [1–8] and computational studies [9–29] has put forward CNTs as promising structural elements for heat management applications and has motivated active exploration of the physical mechanisms responsible for the thermal transport in CNTs. Under conditions when systematic experimental investigation of the dependence of thermal conductivity on the geometrical and structural parameters of CNTs (length, diameter, chirality, curvature, presence of defects) and external conditions (temperature, thermal contact resistance, interactions with other CNTs and/or substrate) is hampered by technical challenges related to the small size of the individual nanotubes and their propensity to form bundles and aggregate into intertwined structures, atomistic molecular dynamics (MD) simulations present an attractive alternative. Indeed, atomistic simulations allow for complete control over the size and structure of the CNTs and have been used in investigations of the dependence of the thermal conductivity on CNT length [12–15,18,20–24,26,28–34], diameter [11–13,18,22–24,26–29,33,35], elastic deformation [25,36–38], buckling [39–41], as well as presence of isotope dopants [18,20,24,33], crystal defects [10,20,33], or chemisorbed molecules [14].

In spite of the ability of MD simulations to fully control the simulated environment and to provide detailed atomic-level information on the mechanisms responsible for the heat transfer in CNTs, the values of thermal conductivity, k, predicted in different MD simulations exhibit surprisingly large divergence even when the simulated system is nominally the same. For example, a sample of MD results obtained for single-walled CNTs of chirality (10,10) at ~300 K is listed in Table 1. The values of k exhibit variability by more than an order of magnitude, casting doubt on the ability

* Corresponding author. Tel.: +1 434 243 3582.
E-mail addresses: salaway@virginia.edu (R.N. Salaway), lz2n@virginia.edu (L.V. Zhigilei).
URL: http://www.faculty.virginia.edu/CompMat/ (Computational Materials Group).

0017-9310/$ - see front matter © 2013 Elsevier Ltd. All rights reserved.
http://dx.doi.org/10.1016/j.ijheatmasstransfer.2013.11.065

Table 1
A sample of values of CNT thermal conductivity predicted in MD studies reported in the literature. All values are for (10,10) single-walled CNTs at ~300 K. The system length is defined as the total length of the computational system used in the simulations. The nomenclature for the names of the interatomic potentials is explained in the text.

Reference	k (W m^{-1} K^{-1})	System length (nm)	Potential	Method	Boundary conditions
Lukes and Zhong [21]	~20–160	5–40	Brenner-II + LJ	EMD	Periodic and non-periodic
Grujicic et al. [16]	~173–179	~2.5–40	AIREBO	EMD	Periodic
Pan [35]	243	~29.4	Brenner-II	NEMD	Periodic
Xu and Buehler [36]	301	49.26	AIREBO	NEMD	Periodic
Wei et al. [37]	302	49.26	AIREBO	NEMD	Periodic
Che et al. [10]	~240–305	~2.5–40	Brenner	EMD	Periodic
Padgett and Brenner [14]	~35–350	~10–310	Brenner-II	NEMD	Periodic
Thomas et al. [26]	~300–365	200–1000	Brenner-II	NEMD	Non-periodic
Maruyama [12]	~275–390	6–404	Brenner	NEMD	Non-periodic
Shiomi and Maruyama [23,42]	~130–475	~14–425	Simplified Brenner	NEMD	Non-periodic
Feng et al. [33]	~50–590	6.52–34.77	Brenner-II	NEMD	Non-periodic
Bi et al. [20]	~400–600	2.5–25	Tersoff	EMD	Periodic
Cao and Qu [28]	1580	4800	Optimized Tersoff	NEMD	Periodic
Ren et al. [25]	~1430	~60	AIREBO	NEMD	Non-periodic
Berber et al. [9]	~6600	~2.5	Tersoff	HNEMD	Periodic

of MD simulations to provide a reliable quantitative estimate of the thermal conductivity. It is important, therefore, to understand the reasons for the data variability across the published studies and, in particular, to evaluate the contributions of two fundamentally different factors: true variation of the intrinsic CNT conductivity due to the variation of length of the CNTs used in the simulations, and variation of k due to variability of computational procedures and interatomic potentials employed in different simulations.

The length dependence of thermal conductivity of CNTs is commonly observed in MD simulations performed for nanotubes with length up to hundreds of nanometers [10,12,14–18,21–24,26,28,29,33]. There are two main reasons for this behavior. First, when the sample length is less than or comparable to the phonon mean free path, phonons are capable of traveling ballistically through the sample without being impeded by phonon–phonon scattering. As the sample length increases, the effective length of this ballistic transport increases, which increases overall thermal transport and results in higher conductivity values. Second, the longest available phonon wavelength that can exist in a CNT is dictated by the sample length. Thus, as the sample length increases, the maximum allowable phonon wavelength increases. The additional long-wavelength phonons offer effective channels for thermal transport and can make a substantial contribution to the thermal conductivity [21,28]. The CNT length that corresponds to the transition from the ballistic conduction regime, where the thermal conductivity increases with CNT length, to the diffusive regime, where the thermal conductivity approaches a constant value, is temperature dependent as the phonon mean free path decreases with increasing temperature. A recent review of room temperature experimental measurements performed for CNTs with length exceeding 0.5 μm [43] suggests the diffusive regime of the heat transfer. At the same time, the results of MD simulations performed for CNTs with lengths of 10s to 100s of nm typically exhibit a pronounced increase of k with increasing CNT length, that is characteristic of the ballistic and transitional diffusive-ballistic phonon transport [12,14,15,18,21–24,26,28,33]. The length dependences predicted in different MD studies, however, vary widely for the same (10,10) CNT, with the transition to the diffusive regime (saturation of k) predicted for as short CNTs as 10 nm in some of the investigations [10,15–17,29], while no saturation is observed for CNTs with length exceeding 1 μm in other studies [23,28]. In order to reconcile the diverging results on the CNT length dependence, the sensitivity of the predictions of MD simulations to the interatomic potential and computational procedures used in the calculations of thermal conductivity has to be systematically evaluated.

The interatomic potential that defines the interaction forces between atoms in the simulated system is a key ingredient of any MD model. The choice of interatomic potential has direct effect on any quantitative prediction of MD simulations, including prediction of the value of thermal conductivity. A sample of results obtained with interatomic potentials commonly used in simulations of CNTs are listed in Table 1. Note that some of the potentials have been modified and different versions and generations of the same potential are concurrently used by different research groups. As a result, there can even be confusion as to the exact version of potential indicated by name in a published work.

For clarity, the following nomenclature convention is defined in this paper. The Tersoff potential is the early bond order potential that has the original functional form and parameterization defined by Tersoff in 1988 [44,45]. The Brenner potential is the potential developed by Brenner in 1990 [46]. Stuart and colleagues modified the Brenner potential, added a description of torsional interactions for rotation about single bonds and developed an adaptive treatment of non-bonded van der Waals interactions within the bond order formalism of the Brenner potential. This potential, described by Stuart et al. in 2000 [47] is referred to as adaptive intermolecular reactive bond order (AIREBO) potential. In 2002, Brenner et al. made changes to the functional form and parameterization of the original Brenner potential to improve the accuracy of the description of hydrocarbon molecules and various properties of diamond [48]. We refer to this second-generation Brenner potential as Brenner-II. A description of van der Waals interactions through simple addition of the Lennard–Jones (LJ) potential to the Tersoff, Brenner, and Brenner-II potentials has also been used in simulations that do not involve formation/dissociation of chemical bonds and do not require adaptive treatment of the intermolecular interactions [21,32,49]. These potentials can be denoted as Tersoff + LJ, Brenner + LJ, and Brenner-II + LJ, and a set of parameters ϵ and σ of the Lennard–Jones potential should be provided to define the combined potentials. New sets of parameters for the Tersoff and Brenner potentials, optimized for the description of phonon thermal transport in carbon nanotubes and graphene, were recently suggested by Lindsay and Broido [50]. We refer to these potentials as optimized Tersoff and optimized Brenner in this paper. Finally, Yamaguchi and Maruyama [51] used a simplified version of the original Brenner potential, in which the conjugate-compensation term is eliminated to facilitate the formation of poly-cyclic structures in simulations of fullerene formation process. This implementation was used by Shiomi and Maruyama [23] in simulations of thermal conductivity of CNTs and is referred to as simplified Brenner in this paper.

Another factor that may be responsible for the inconsistency of the computational predictions is the variability of the methods employed for the calculation of thermal conductivity in MD

simulations. Two general types of methods are used in the analysis of thermal transport properties. In the equilibrium molecular dynamics (EMD) method, small fluctuations of heat current are monitored over time and Green–Kubo relation is used to determine the thermal conductivity from these perturbations from equilibrium [10,16,20,21]. While periodic boundary conditions are often used in EMD calculations to represent an infinitely long CNT [9,52], the results of the calculations show an increase in the conductivity with increasing length of the computational cell [10,16,17,21,29,32].

In the non-equilibrium molecular dynamics (NEMD) method, a steady-state temperature gradient is created between "heat bath" regions defined in the system and the thermal conductivity is determined from the Fourier law. The heat flux can be applied directly or indirectly by prescribing either the energy flux or temperature gradient. The NEMD studies referenced in Table 1 provide examples of the different approaches to creating a temperature gradient. In particular, Thomas et al. [26] and Cao and Qu [28] directly applied an energy flux by removing a known amount of kinetic energy from a cold heat bath region in a CNT and adding it to a hot heat bath region to impart a flux between the two regions. Maruyama [12], Shiomi and Maruyama [23], Feng et al. [33], and Ren et al. [25] directly applied the temperature gradient by fixing the temperatures of the heat bath regions on both sides of the CNT. Finally, Pan [22], Xu and Buehler [36], Wei et al. [37], and Padgett and Brenner [14] indirectly applied a heat flux by periodically exchanging the momenta between the slowest atom in the hot heat bath region and the fastest atom in the cold heat bath region. The boundary conditions applied at the ends of the computational system are also varied across NEMD simulations and include free boundary conditions applied to CNTs ends [18,31], rigid boundary conditions with heat bath regions immediately adjacent to the fixed ends of the CNT [26,33,40] or separated from the fixed ends by an intermediate layer [25,53], and periodic boundary conditions applied along the axis of the CNT [11,14,15,24,28,35–37]. In the case of the periodic boundary conditions, the distance between the centers of the hot and cold heat bath regions has to be twice shorter than the total length of the computational domain to satisfy the requirement of periodicity of the temperature distribution.

The diversity of methods and types of boundary conditions results in the ambiguity of the definition of the CNT length. In the EMD method, there are no heat bath regions, and the computational cell can be considered to represent the actual CNT length if free boundary conditions are used [21] or an infinite CNT in the case of periodic boundary conditions, with longer cells providing a more accurate representation [17]. In the NEMD method, when the heat bath regions are employed, it is common to consider the CNT length to be the unperturbed length between the two heat bath regions [23,26,30,38]. However, the thermally controlled regions can also be included in the definition of CNT length, particularly in works employing the NEMD method with periodic boundary conditions [14,15,28]. Furthermore, in the case when the periodic boundary conditions are used, the CNT length can be defined as the overall length of the computational cell [15,22,36] or the twice shorter distance between the centers of the heat bath regions [24,28]. This variation in CNT length definitions is addressed below in further detail. For the purposes of Table 1, the system length refers to the length of the entire computational domain for all works.

The brief review of computational work provided above suggests that the results of the MD calculations of thermal conductivity are significantly affected by the choice of interatomic potential, computational method, boundary conditions, and definition of the effective CNT length. While the sensitivity of the predictions of MD simulations to the choice of the computational setup is generally recognized [21,26,28,32,37,43], there has been no targeted studies aimed at systematic evaluation of the relative effect of various computational parameters on the CNT conductivity values. Understanding of the extent to which the computational parameters affect the predicted values of thermal conductivity is necessary not only for resolving the discrepancies in the reported results of MD studies, but also for investigation of any real effects of the CNT length or physical environment, in isolation of any artifacts of the computational setup. Therefore, in this work, we perform several series of simulations that are specifically designed to evaluate the effects of the boundary conditions, size and location of the heat bath regions, definition of the CNT length, and the choice of interatomic potential on the predictions of NEMD simulations. General features of the computational setups used in the simulations are described in Section 2 and the results of the simulations are presented and discussed in Section 3.

2. Computational method

Simulations are designed to predict the thermal conductivity of individual (isolated) CNTs. While some procedures are varied across different series of simulations, the basic sample preparation and computational procedure is common to all of the simulations and is outlined below.

Simulations are performed for individual (10,10) CNTs covered by 110-atom caps at the ends, with one of the caps interfacing with the CNT by a 20-atom ring constituting a half of the nanotube's unit cell. Free (vacuum) boundary conditions are applied in all directions. Initially, all CNTs undergo relaxation for 25 to 100 ps in constant energy MD simulations. Next, the CNTs are gradually heated up to 300 K over the course of 20 to 50 ps using the Langevin thermostat method [54], while ensuring that the total linear and angular momenta of the CNTs are zero [21]. After the heating process, an additional 20 ps relaxation in constant-energy free dynamic simulations is employed to monitor the CNT system coordinates and energies, and to verify that mechanical-vibrational equilibration is achieved after the temperature increase.

The thermal conductivity of CNTs is determined in NEMD simulations by generating constant heat flux between hot and cold bath regions defined in the CNTs. The heat flux is applied by adding a fixed amount of energy at a constant rate through scaling the velocities of atoms in the heat bath regions so that the same amount of energy Q is added and removed per unit time in the hot and cold heat bath regions, respectively. This creates a constant one-dimensional heat flux, $q = Q/\Omega$, between the heat bath regions, where Ω is the cross-sectional area of the CNT, defined in this work as $\Omega = 2\pi\delta_T R_T = 1.43\ \text{nm}^2$, $R_T = 0.67$ nm is the nanotube radius found in MD simulations as the average radial distance of carbon atoms from the axis of an isolated CNT equilibrated at 300 K, and $\delta_T = 0.34$ nm is the nominal thickness of the CNT wall taken to be equal to the interlayer spacing in graphite [12,41,55].

The applied flux creates a non-equilibrium temperature profile in the sample, which is determined by the flux and conductivity of the CNT. The temperature profile is obtained by dividing the nanotube into segments and calculating local temperature of each segment from the average kinetic energy of the corresponding atoms,

$$T_j = \frac{1}{3k_B N_S}\sum_{i\in S_j} m v_i^2, \tag{1}$$

where T_j is the temperature of segment j, N_S is the number of atoms in a segment, v_i is the instantaneous velocity of atom i, m is the atomic mass, k_B is the Boltzmann constant, and the summation is performed over atoms that belong to segment j. A representative temperature profile generated for a 630 nm CNT, divided into ~24.2 nm segments is shown in Fig. 1. The bath regions were 0.5 nm wide, and positioned ~1 nm from the extreme ends of the tube, to exclude the fullerene caps. The temperature gradient,

dT/dx, is determined from a linear fit applied to the temperature profile, with non-linear parts of the temperature distribution adjacent to the heat bath regions excluded from the fitting procedure.

Once the temperature gradient is found, the CNT conductivity can be calculated from the Fourier law, $k = -q/(dT/dx)$. One of the most important requirements of the NEMD method is to ensure that the system has reached the steady state. During the time of the simulation with the flux implemented, the temperature gradient evolves from zero to the final steady-state value. Measuring the temperature gradient before steady-state temperature profile is established will result in an over-prediction of the CNT conductivity. To ensure the system has reached the steady state, a moving average of thermal conductivity over a fixed temporal window is monitored. Temperature profiles are averaged over the moving time window throughout the simulation and a moving temporal average of the conductivity is obtained. The evolution of the conductivity averaged over the moving time interval is used to determine when the steady-state temperature gradient is established in the system. All data for times after the steady state was reached are averaged in calculation of the final value of thermal conductivity.

A representative temporal conductivity plot calculated for the same 630 nm long CNT used for the illustration of the temperature profile in Fig. 1 is shown in Fig. 2. In this example, data was recorded every 0.005 ps and averaged over a 100 ps temporal window. The initial values of thermal conductivity calculated at the start of the constant heat flux simulation are much higher than the final values, and are not shown in this figure. As the simulation progresses, the conductivity decays to a steady-state value. After 3250 ps, the temporal decay of conductivity ceases and the temporal variation of the conductivity values can be attributed to statistical fluctuations about an average value. The final value of the thermal conductivity is obtained by averaging over the steady-state part of the simulation as schematically shown by the horizontal arrow in Fig. 2.

All simulations reported in this paper are performed with the LAMMPS package [56]. The equations of motion are solved using the velocity Verlet algorithm and the timestep of integration is 0.5 fs. In the simulations presented in Sections 3.1, 3.2, and 3.3, interatomic interactions are described with the LAMMPS implementation of the AIREBO potential [47] that adopts the Brenner-II potential [48] for chemically bonded carbon atoms and describes the van der Waals interactions between non-bonded carbon atoms by the Lennard–Jones potential with parameters $\sigma = 3.40$ Å and $\epsilon = 2.84$ meV. A cutoff function that ensures a smooth transition of the Lennard–Jones potential to zero is applied in a range of interatomic distances from 2.16σ to 3σ. In Section 3.4, the effect of the choice of interatomic potential on the value of thermal conductivity predicted in NEMD is analyzed by performing additional simulations with Tersoff [45], Brenner-II [48], LAMMPS implementation of AIREBO [47], and optimized Tersoff [50] potentials.

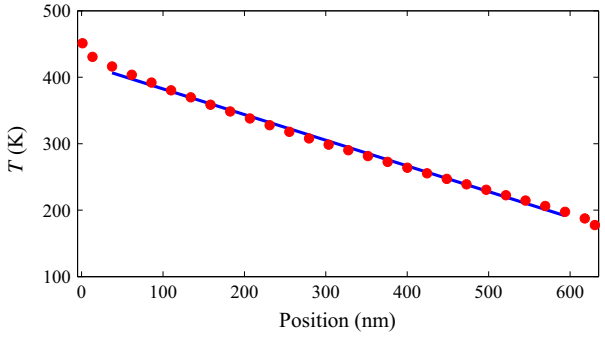

Fig. 1. A representative steady-state temperature profile obtained in a simulation performed for a 630 nm long (10,10) CNT. The data points are calculated for ~24.2 nm segments along the CNT. The line is a linear fit that is used in the calculation of the temperature gradient. The fit excludes the data points that correspond to the heat bath regions and first points adjacent to the heat bath regions.

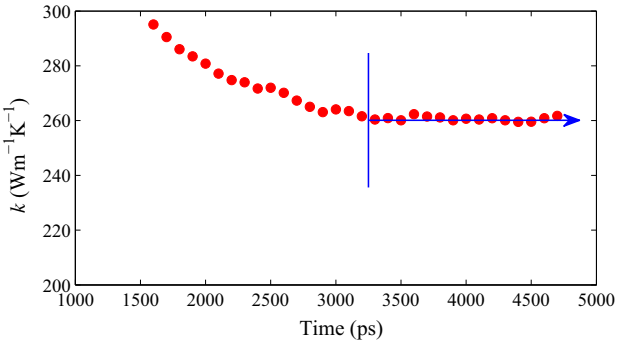

Fig. 2. A representative plot of the time evolution of thermal conductivity, k, calculated from temperature profiles averaged over a moving 100 ps temporal window in a simulation of heat flow through a 630 nm long (10,10) CNT. The heat flux is applied starting at the time of 65 ps and the steady state is deemed to be reached by the time of 3250 ps (marked by the vertical line). The final value of k is determined by averaging all data obtained within the time interval indicated by the horizontal arrow.

3. Results and discussion

The results of a systematic evaluation of the sensitivity of the values of thermal conductivity predicted in NEMD simulations to the computational parameters commonly varied in past investigations are reported in this section. The effect of the CNT length is evaluated first, followed by the analysis of the sensitivity of the computational predictions to the size and location of the heat bath regions and the choice of interatomic potential.

3.1. Effect of CNT length

A series of simulations was performed to examine the length dependence of CNT conductivity. The CNT length was varied between 47 and 630 nm (8240 to 104,440 atoms, respectively). Following a common convention adopted in many NEMD studies of thermal conductivity, e.g., [23,26,30,31,38,57,58], we define the CNT length to be equal to the length of a central unperturbed part of the tube, L_C, located between the 0.5 nm wide hot and cold heat baths regions. The results of the calculations of thermal conductivity plotted as a function of L_C are shown in Fig. 3. The strong length dependence observed for CNTs shorter than ~200 nm suggests the dominant contribution from ballistic phonon transport. For lengths greater than ~200 nm, the dependence on CNT length becomes weaker. This marks the transition to the diffusive-ballistic regime and indicates that the sample length that corresponds to the onset of this transition is on the order of the effective phonon mean free path [59]. Note that the extent of the transitional diffusive-ballistic regime is defined by the longest mean free paths of long-wavelength phonons (of the order of several μm at room temperature [60]) that dominate the heat transfer in CNTs. Thus, while the dependence predicted in our simulations becomes notably weaker and shows signs of saturation as the length increases to 630 nm, the gradual increase of the thermal conductivity with increasing length may be expected up to CNT lengths of the order of tens of μm [61,62].

For comparison, the results of other NEMD studies that report CNT length dependence of thermal conductivity [14,21,23,26] are also plotted in Fig. 3. While the predicted values of conductivity vary across these works, the qualitative trends in the length

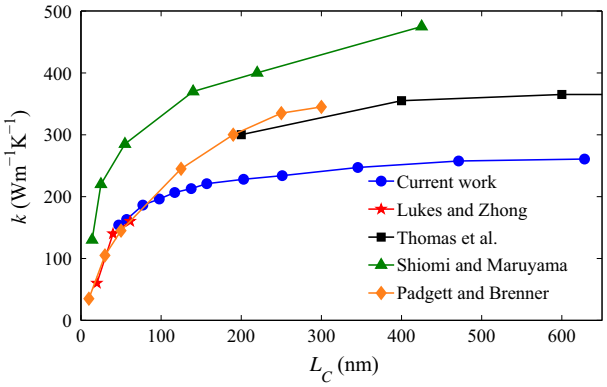

Fig. 3. Thermal conductivity, k, of (10,10) CNTs as a function of sample length, L_C, defined as the distance between the hot and cold heat bath regions. For comparison, the length dependencies of thermal conductivity reported by Lukes and Zhong [21], Thomas et al. [26], Shiomi and Maruyama [23], and Padgett and Brenner [14] are also plotted. While quantitative discrepancies are present, all sets of data exhibit a consistent trend of strong length dependence for short CNTs transforming to weaker increase for CNTs that are longer than ~200 nm, thus signifying the transition from the ballistic to diffusive-ballistic heat transport regimes.

dependencies are similar. For CNTs with lengths shorter than 200 nm, all studies predict a strong length dependence of the conductivity, characteristic of dominant ballistic thermal transport. In studies where CNTs longer than 200 nm are investigated, a transition to a weaker length dependence and saturation of the conductivity values with increasing nanotube length is observed, suggesting a transition to the diffusive-ballistic regime. The transition between the two regimes is observed for nanotube length that roughly corresponds to the room temperature phonon mean free path that has been estimated to be of the order of 200–500 nm based on experimental data [1,4], results of recent NEMD simulations [28] and theoretical analysis [59].

The strong sensitivity of the thermal conductivity to the CNT length predicted in NEMD simulations demonstrates that quantitative comparison between the results of different simulations should account for the length dependence, especially when the results are compared for short CNTs, in the ballistic heat transport regime. Apart from the length dependence, the factors responsible for the apparent quantitative discrepancies in data obtained in different simulations illustrated in Fig. 3 are investigated and discussed below.

3.2. Effect of the length of heat bath regions

The results summarized in Fig. 3 demonstrate large discrepancies in quantitative results obtained in different studies. It is reasonable to assume that the differences in the computational setups used in different studies are to blame for the discrepancies in the results. There have been no systematic studies, however, reported on the effect of various parameters on the values of thermal conductivity predicted in NEMD simulations. Therefore, the remainder of this paper describes the results of several series of simulations targeted specifically at revealing the effect of some of the key simulation parameters on the predictions of CNT thermal conductivity. The conclusions of this study provide both insights into the nature of the nanoscale thermal transport in CNTs and recommendations on the choice of the computational parameters that may lead to the reduction in the discrepancies between the results of different simulations.

When employing the NEMD method described in Section 2 to study thermal conductivity of CNTs in the ballistic regime, the length of the two heat bath regions, $2L_B$, can account for a substantial portion of the overall system length, L_{Sys}, as measured from end to end, Fig. 4. In most NEMD studies employing non-periodic (rigid or free) boundary conditions, however, the CNT length is defined as the length between the inner boundaries of the heat bath regions, or the length of the central part of the nanotube, L_C, e.g., [23,26,30,31,38,57,58]. This definition of sample length is not limited to CNTs but is commonly applied in NEMD investigations of various materials [63–65]. The effect of the length of the heat baths is implicitly assumed to be negligible in most of these studies employing this definition of sample length. This assumption is challenged, however, by the results of two studies [23,30] where the effect of L_B on k is analyzed. The simulations performed for CNTs with fixed size of the central region L_C but varied length L_B of Nose–Hoover thermostats applied to the heat bath regions demonstrate that the value of k has a pronounced dependence on L_B.

Shiomi and Maruyama [23] attributed this behavior to a thermal boundary resistance (TBR) present between each of the heat bath regions and the central tube region. According to this explanation, a difference between the bath length and the central tube length results in a difference in allowable phonon states in each of these regions. This mismatch in phonon states, and the resulting TBR, cause an abrupt temperature change at the interface between the central and heat bath regions, and thus affect the final steady-state temperature gradient used in the calculation of the conductivity. They concluded that this effect can be minimized when the length of the heat bath regions is equal to the central tube length, *i.e.*, $L_B = L_C$. Based on this conclusion, Shiomi and Maruyama suggest that a bath region with length equal to half the length of the central tube region, $L_B = L_C/2$, should be used as an optimal choice that ensures a sufficient reduction of the TBR effect at a reasonable computational cost.

To further examine the effect of the length of the heat bath regions, we performed two series of NEMD simulations. In both series we use (10,10) CNTs covered by fullerene caps at the two ends. In the first series, Series 1, the distance between the heat bath regions was fixed at $L_C = 50$ nm while the length of each heat bath region was varied within a range from $L_B = 0.5$ nm to $L_B = 75$ nm. In the second series of simulations, Series 2, the central tube length was fixed at $L_C = 97$ nm and the length of the heat bath regions was varied from $L_B = 25$ nm to $L_B = 150$ nm. The two sets of parameters are chosen to allow for analysis of the effect of the length of the heat bath regions for the conditions when the bath regions are both shorter and longer than the central parts of the nanotubes. The calculations of the thermal conductivity follow the general procedure described in Section 2. The heat flux is maintained by adding/removing the kinetic energy in the heat bath regions at rates of Q = 0.45 eV/ps for $L_C = 50$ nm (Series 1) and Q = 1.25 eV/ps for $L_C = 97$ nm (Series 2).

Additional analysis was performed to estimate the standard error of the mean conductivity. After achievement of the steady state, calculations of conductivity are continued for an additional 2500 ps for Series 1 and 500 ps for Series 2. For each simulation, the data obtained in the steady state are divided into N sample sets, each with M conductivity calculations. The sample mean of each sample set, k_i, is calculated to provide N estimations of the true

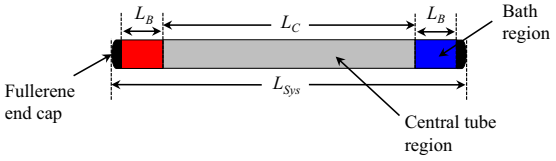

Fig. 4. A schematic of a computational setup used in NEMD simulations of thermal conductivity of CNTs and the definitions of the length parameters. Two heat bath regions of length L_B are separated by a central tube region of length L_C.

mean conductivity predicted in the NEMD simulation. The final value of the conductivity reported is the mean of the N estimations, $\overline{k}$. Averaging over M measurements in each sample set reduces the effect of the natural statistical fluctuations in instantaneous temperature profiles that arise due to the relatively small number of atoms in each CNT segment and provides a more accurate estimation of the mean conductivity. This method produces a sample of N independent estimations of the mean conductivity and is used to estimate the standard error of the mean [66]. The sample standard deviation, S, is determined as

$$S = \left(\frac{1}{N} \sum_{i=1}^{N} (k_i - \overline{k})^2 \right)^{1/2}, \quad (2)$$

and the estimated standard error of the mean is calculated as $\hat{\sigma}_{\overline{k}} = S/\sqrt{N}$. This value provides a measure of the precision in estimating the mean conductivity predicted by the NEMD simulations.

The results of the two series of simulations plotted as a function of L_B are shown in Fig. 5. The data represented by green triangles are the results for Series 1, where the central tube length was $L_C = 50$ nm, and the data represented by red squares are the results for Series 2, where the central tube length was $L_C = 97$ nm. The error bars represent the estimates of the standard error of the mean conductivity predicted in the simulations. In both series of simulations, the conductivity shows a strong dependence on the length of the heat bath regions. The values predicted in the simulations range from 165 W m^{-1} K^{-1} to 229 W m^{-1} K^{-1} and from 220 W m^{-1} K^{-1} to 256 W m^{-1} K^{-1} for Series 1 and Series 2, respectively. These are significant variations, particularly in light of the common practice of defining CNT length as the distance between the inner boundaries of the two heat bath regions and the lack of a rigorous criterion for choosing the length of the heat bath regions. In the case of Series 1, for example, the results imply up to 39% variation in the conductivity values predicted for a 50 nm CNT, depending on the choice of the length of the heat bath regions, L_B.

It is also instructive to compare the results of the two series of simulations performed with fixed values of L_C with the data used in Section 3.1 to examine the length dependence of k. In this additional series of simulations, Series 3, the length of the heat bath regions was kept constant at $L_B = 0.5$ nm, and L_C was varied from 47 nm to 630 nm. In Fig. 6(a), all data is plotted as a function of L_C, which is a standard way to define the CNT length in the NEMD length dependence studies employing non-periodic boundary conditions [23,26,30,31,38,57,58]. In this representation, we can see that the variations of the values of k in the constant L_C series (Series 1 and 2) are comparable to the range of values obtained by changing L_C in Series 3.

Perhaps a more significant aspect of Fig. 5 is that the values of thermal conductivity predicted in the Series 1 and 2 simulations continue to increase with increasing lengths of the heat bath regions even for $L_B > L_C$. The solid green and dashed red lines in Fig. 5 mark the values of k predicted in simulations of Series 1 with $L_B = L_C = 50$ nm and Series 2 with $L_B \approx L_C$ ($L_B = 100$ nm, $L_C = 97$ nm), respectively. According to the interpretation offered by Shiomi and Maruyama [23], TBR between the heat bath regions and the central region of the unconstrained dynamics should reach a minimum for $L_B = L_C$ and the thermal conductivity should not increase with further increase of the heat bath length. The continued increase in the conductivity for the bath lengths $L_B > L_C$ suggests that the interpretation based on the TBR caused by the mismatch of the vibrational spectra of the heat bath regions and the central part of the CNT has to be reconsidered.

The results of the present simulations suggest that the length dependence of thermal conductivity predicted in NEMD simulations is most adequately described as the dependence on the overall (end-to-end) length of the system, L_{Sys}. The nature of this dependence is illustrated in Fig. 6(b), where the exact same data from Fig. 6(a) is re-plotted as a function of the overall system length, L_{Sys}. A striking observation from this plot is that when the

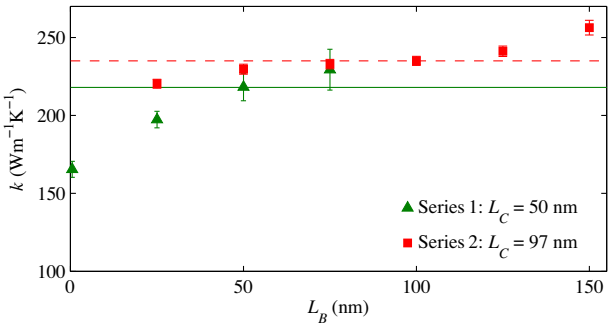

Fig. 5. Thermal conductivity, k, as a function of the length of the heat bath regions, L_B. The results are shown for two series of NEMD simulations performed with fixed distance between the heat bath regions: in Series 1 (green triangles) $L_C = 50$ nm and in Series 2 (red squares) $L_C = 97$ nm. The error bars show the estimates of the standard error of the mean, with some error bars obscured by the width of the data points. The solid green and dashed red lines mark the values of k predicted in simulations of Series 1 with $L_B = L_C = 50$ nm and Series 2 with $L_C \approx L_B = 100$ nm, respectively. The consistent trend of increasing thermal conductivity for $L_B > L_C$ contradicts the notion that the sensitivity of the results to L_B is due to the thermal boundary resistance at the boundaries of the heat bath regions. (For interpretation of the references to color in this figure caption, the reader is referred to the web version of this article.)

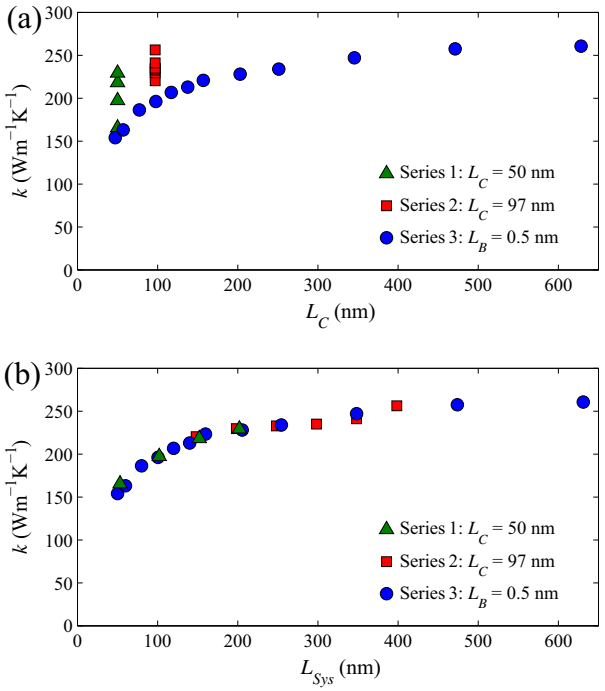

Fig. 6. Thermal conductivity, k, as a function of (a) length of the central part of the CNT, L_C, and (b) the total length of the CNT, L_{Sys}. The results are shown for three series of NEMD simulations: in Series 1 (green triangles) CNTs have fixed $L_C = 50$ nm and varied L_B, in Series 2 (red squares) CNTs have fixed $L_C = 97$ nm and varied L_B, and in Series 3 (blue circles) CNTs have fixed $L_B = 0.5$ nm and varied L_C. While it is common to use L_C as a measure of the effective CNT length in NEMD simulations of thermal conductivity, plotting k versus L_{Sys} in (b) provides a more consistent representation of the length dependence of k across all series of simulations, regardless of whether the length is added to the central region (Series 3) or the bath regions (Series 1 and 2) of the nanotube. (For interpretation of the references to color in this figure caption, the reader is referred to the web version of this article.)

results from the three series of simulations are plotted with respect to L_{Sys}, the effect of increasing L_B in Series 1 and 2 is nearly *indistinguishable* from the effect of increasing L_C in Series 3. A near coincidence of the three points at $L_{Sys} \approx 200$ nm in Fig. 6(b) is a good illustration of this observation. The similarity of the values of k predicted in the three series of simulations and listed in Table 2 is consistent with the notion that the overall system length determines the value of the thermal conductivity. These CNTs, however, would be considered to have very different lengths by the common definition of CNT length as the length of the central part of the nanotube, L_C.

The length dependence of the thermal conductivity obtained in the simulations can be extrapolated to samples of infinite length to obtain an estimate of the thermal conductivity, k_∞. From the kinetic theory for a phonon gas, the thermal conductivity can be related to the phonon mean free path as

$$k = \frac{1}{3} c v l_{eff}, \tag{3}$$

where c is the phonon heat capacity per unit volume, v is the average phonon velocity, and l_{eff} is the effective mean free path of the phonons. In a CNT of a finite length, the effective mean free path is defined by both the phonon–phonon scattering and the phonon scattering at the boundaries of the CNT. Using Matthiessen's rule for independent contributions of the two scattering mechanisms, the effective mean free path can be written as

$$\frac{1}{l_{eff}} = \frac{1}{l_\infty} + \frac{2}{L_{Sys}}, \tag{4}$$

where l_∞ is the mean free path of phonons in the system where $L_{Sys} \to \infty$. From Eqs. (3) and (4), it follows that the length dependence of the thermal conductivity can be written as [67,68]

$$\frac{1}{k} = \frac{M}{2l_\infty} + \frac{M}{L_{Sys}}, \tag{5}$$

where M is a constant that defines the slope of the linear dependence of $1/k$ on $1/L_{Sys}$. The estimates of the phonon mean free path and thermal conductivity in an infinitely long CNT, l_∞ and k_∞, can then be obtained by plotting the dependence of $1/k$ on $1/L_{Sys}$ predicted in NEMD simulations and extrapolating it to $L_{Sys} \to \infty$. Note that this linear extrapolation procedure provides only the first order approximation of the values l_∞ and k_∞. The variability of the phonon group velocities and mean free paths [60], neglected in the simple equation (3), may result in substantial deviations from the linear dependence of $1/k$ on $1/L_{Sys}$ [26,65]. However, a linear relationship was observed for the range of system lengths investigated in this work.

The values of l_∞ and k_∞ obtained by the procedure outlined above for the three series of simulations are listed in Table 3. The conditions of simulations of Series 3, where the size of the heat bath regions is kept constant while L_C is increased, are the closest reflection of the true physical system of interest. Thus, one can expect that the most accurate prediction of k_∞ would come from the application of the extrapolation procedure to data produced in this series. The extrapolation of data from Series 1 and 2, where L_C is kept constant and L_B increases, can be represented by a CNT with a fixed length of the central part of the nanotube, but infinitely-long bath regions. It is clear that this representation does not match the true physical system of interest when considering the conductivity of infinite systems. While the highest prediction comes from extrapolation of the results of Series 3, it can be seen that the extrapolated values for $L_B \to \infty$ are similar to the one obtained for $L_C \to \infty$ and the agreement improves as L_C increases from 50 nm to 97 nm.

Table 2
Sample data taken from Fig. 6. Overall system length, L_{Sys}, which includes the heat bath regions, is found to be a better predictor of conductivity than the distance between the heat bath regions, L_C.

	k (W m^{-1}K^{-1})	L_{Sys} (nm)	L_C (nm)
Series 1	229	202	50
Series 2	230	198	97
Series 3	228	206	203

Table 3
The upper saturation limit of conductivity, k_∞, and phonon mean free path, l_∞, predicted by fitting the results of NEMD simulations to Eq. (5). The values of L_C and L_B correspond to systems extrapolated to infinite overall length, L_{Sys}, by following the procedures of the three series of simulations. Series 3 provides the most realistic representation of the true system of interest, with length added to the central region of the nanotube. Despite length being added to the heat bath regions while L_C is kept constant, Series 1 and 2 provide estimates of k_∞ that are surprisingly close to the more realistic prediction of Series 3.

	L_C (nm)	L_B (nm)	k_∞ (W m^{-1} K^{-1})	l_∞ (nm)
Series 1	50	∞	263	16
Series 2	97	∞	267	16
Series 3	∞	0.5	275	20

The main conclusion drawn from Fig. 6 is that the length dependence of CNT conductivity is better captured by the overall system length, L_{Sys}, than by the length of the central part of the nanotube, L_C. The length of the heat bath, L_B, is shown to have a strong effect on the values of k predicted in NEMD calculations for CNT lengths comparable to the phonon mean free path. This length dependence is nearly indistinguishable from the dependence on L_{Sys} and the agreement improves as L_C increases from 50 nm to 97 nm. This suggests that the contribution to thermal conductivity from L_B is similar to the contribution from L_C. It follows that bath regions of any significant length should be considered to be parts of the nanotube, and the CNT length should be defined as the length of the overall system, L_{Sys}. Physically, these results imply a relatively minor contribution of the phonon scattering at the interface between the heat bath regions and the unperturbed region of the system to the overall length dependence of the thermal conductivity. The dominant contribution is coming from the real boundaries of the sample, which scatter phonons and limit the maximum phonon wavelength that can exist in the nanotube.

Although the length dependencies shown in Fig. 6(b) for the three series of simulations are similar, the extrapolated values obtained by increasing L_B do not exactly reproduce the values obtained by increasing L_C, as seen in Table 3. Therefore, the choice of a small bath length would be optimal for obtaining an accurate prediction of the length dependence of k and the extrapolated value of k_∞. Overall, the results of the analysis discussed above provide guidance for choosing a simulation setup that best represents the conductivity of a system of interest. CNT length definition should *include* the heat bath regions, and the length of the heat bath regions should be small compared to the total length of the system. It is worth noting that the underlying physics of the effects of thermal bath length is applicable to phonon thermal transport in the ballistic-diffusive length regime of any material. Thus, this definition of CNT length can be extended to the definition of sample length in any NEMD study of thermal transport.

3.3. Effect of location of heat bath regions

The variation of computational setups used for the generation of steady-state heat fluxes in NEMD simulations could be an additional source of the discrepancies in the computational predictions. There are two commonly used ways of implementing the heat flux. In all simulations discussed above, the temperature or heat flux control is applied to the two heat bath regions located at the ends

of a CNT and a steady-state heat flux is created in the central part of the CNT, between the two heat bath regions. Fig. 4 represents a schematic of this computational setup. This method of applying a uni-directional heat flux along the length of the sample is used in a number of works [12,13,18,19,23,25–27,30–33,38,40,57,58,69,70]. An alternative implementation of the NEMD method is represented in Fig. 7. In this approach, a hot heat bath region is defined in the center of the tube, two cold heat baths regions are applied at the two ends of the CNT, and equal and opposite fluxes are generated along the tube axis in opposite directions. This implementation is typically used in combination with periodic boundary conditions (PBCs) in the axial direction [11,14,15,22,24,28,35–37], thus creating a repeating pattern of bi-directional fluxes.

The discussion provided in the previous section demonstrates that for NEMD simulations implementing uni-directional flux, the length dependence of CNT conductivity is better captured by the overall system length, L_{Sys}, than by the length between the heat bath regions, L_C, although the majority of studies employing this method to investigate length dependence of conductivity use L_C as the defining length [23,26,30,31,57,58]. Paradoxically, the results obtained in bi-directional flux simulations are often described in terms of the overall system length as the defining length [15,22,36,37], despite the imposed thermal transport occurring in opposite directions over the two halves of the system length. This length definition does not seem to be intuitive given the nature of thermal transport in these systems, and the factors that affect the length dependence in the ballistic and diffusive-ballistic regimes. When a flux is applied between two heat bath regions, the dominant ballistic transport mechanism is energy transport from a hot heat source to a cold heat sink. In the case of bi-directional heat flux, the ballistic transport contributes to the heat transfer between the hot and cold bath regions, in the direction of the imposed heat flux. If the phonon mean free path is longer than the distance between the heat bath regions, however, the thermal transport may occur from a heat source, *through* a heat sink, and toward the second heat source on the other side of the computational system, against the dominant direction of heat transfer. In this case, the ballistic transport would actually serve to reduce the measured temperature gradient and the corresponding thermal conductivity, as it effectively inhibits the heat transfer in the direction of imposed flux. Thus, the ballistic thermal transport within the distance between the heat baths serves to increase thermal conductivity, while the ballistic transport at lengths greater than the distance between the heat baths regions serves to reduce the conductivity. Therefore, it seems plausible that thermal conductivity predicted in NEMD simulations is defined by the length of consistently imposed flux, *i.e.*, the length between the heat bath regions, rather than by the overall system length.

To investigate the effect of the bi-directional flux configuration on the predicted values of thermal conductivity, two NEMD simulations are performed for free and periodic boundary conditions

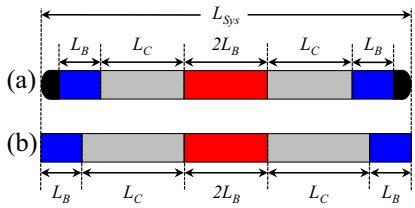

Fig. 7. Schematics of computational setups with bi-directional heat flux implementations used in NEMD simulations of thermal conductivity of CNTs. The two setups are shown for free (a) and periodic (b) boundary conditions. In the case of free boundary conditions, the CNTs are covered by hemispherical fullerene caps that are not included in the heat bath regions.

applied along the axis of the CNTs as shown schematically in Fig. 7. In the case of free boundary conditions, the CNT is covered by two hemispherical fullerene caps and the total length of the system was 100 nm. Two cold bath regions are implemented immediately adjacent to the fullerene caps, and have a length of $L_B = 1$ nm each. A hot bath is implemented in the center of the CNT, measuring $2L_B = 2$ nm. The distance of unperturbed length between the heat bath regions is $L_C = 47.3$ nm on each side of the CNT. In the second simulation, the fullerene caps are removed and periodic boundary conditions are applied in the axial direction, creating a repeating pattern of bi-directional heat flux. In this case the overall system length remains 100 nm, and the distance between the heat bath regions is increased to $L_C = 48.1$ nm to account for the removal of the fullerene caps.

Thermal conductivity is calculated from the steady-state temperature profiles established in the system following a procedure similar to the one described in Section 2. The values of k are found to be 154 W m^{-1} K^{-1} in the free boundary conditions simulation, and 160 W m^{-1} K^{-1} with periodic boundary conditions. Comparing these predictions to the results obtained with uni-directional heat flux approach and described in Sections 3.1 and 3.2, we find that the results of bi-directional calculations are in a good agreement with the ones obtained in simulations of Series 3 for $L_{Sys} = 50$ nm, 154 W m^{-1} K^{-1}, but significantly under-predict the results for $L_{Sys} = 100$ nm, 196 W m^{-1} K^{-1}, see Table 4. This observation supports the qualitative discussion provided above, which suggested that, due to the physical phenomena that lead to the length dependence, the length of consistently imposed heat flux is the length that defines the value of the thermal conductivity in bi-directional NEMD simulations. Keeping in mind the conclusion of Section 3.2, it is reasonable to include the length of the heat bath regions to the standard length definition. Thus, by defining the effective CNT length in bi-directional simulations as the length of an unperturbed region plus $2L_B$, $L_C + 2L_B \approx L_{Sys}/2$, we can reconcile the results obtained with the two types of the computational setup. Adopting this definition of CNT length may help to resolve some of the discrepancies in the values of CNT thermal conductivity reported in the literature.

3.4. Effect of interatomic potential

The interatomic potential is the most significant input parameter that must be defined in any MD simulation. Potentials that have been validated and widely used to represent carbon systems include the Tersoff [45], Brenner [46], Brenner-II [48], and AIREBO [47] potentials. Recently, modified sets of parameters for the Tersoff and Brenner-II potentials have been developed specifically for simulations of heat transfer in carbon nanotubes and graphene [50]. Considering the results of the simulations listed in Table 1, it is possible to see a correlation between the type of interatomic potential employed in a simulation and the values of the predicted thermal conductivity: the increasing values of k tend to follow the order from AIREBO and Brenner-II + LJ, to Brenner/Brenner-II, to Tersoff, and to an optimized version of the Tersoff potential. Here we note two exceptions from this trend: the value reported by Ren et al. [25], which is unusually high in comparison to other works employing the AIREBO potential, and the one by Berber et al. [9] which is acquired with the homogenous non-equilibrium molecular dynamics (HNEMD) routine [71] and remains among the highest reported values in the literature. The differences in the CNT lengths and various parameters of the computational methods employed in the simulations, however, do not allow us to translate this apparent correlation to a definite quantitative conclusion on the extent the choice of the interatomic potential affects the value of thermal conductivity predicted in a simulation. Therefore, an additional series of NEMD simulations is performed in this work

Table 4
Thermal conductivity of (10,10) CNTs, k, predicted in NEMD simulations performed with bi-directional and uni-directional heat flux implementations. The predictions of the two types of simulations are reconciled when the results are compared for the same effective length defined as $L_C + 2L_B$.

Flux direction	Boundary conditions	L_{Sys} (nm)	$L_C + 2L_B$ (nm)	k (W m^{-1} K^{-1})
Bi-	Periodic	100	50	160
Bi-	Free	100	49	154
Uni-	Free	50	49	154
Uni-	Free	100	99	196

for identical CNTs and computational setups, but different interatomic potentials. In this way, the possibility of other system parameters causing divergent results is eliminated, and the pure effect of the interatomic potential is examined in isolation.

The system used in this series of simulations is a (10,10) CNT with uni-directional heat flux (Fig. 4), $L_{Sys} = 205$ nm, and $L_B = 0.5$ nm. The computational setup and procedure used in the calculation of k are the ones described in Section 2. The four potentials investigated are original Tersoff [45], Brenner-II [48], AIREBO [47] with Brenner-II [48] adopted for bonding interactions, and the optimized Tersoff by Lindsay and Broido [50].

The results from the simulations, shown in the form of a bar chart in Fig. 8, reveal strong dependence of CNT conductivity on implemented potential. The general trend is the same as seen in the sample of published results presented in Table 1 (excluding the two highest values reported by Ren et al. [25] and Berber et al. [9]), with the highest values predicted with the optimized Tersoff potential, followed by the original Tersoff, Brenner-II and AIREBO potentials. The low values of k predicted with Brenner-II and AIREBO potentials have been attributed to two factors: low velocities of acoustic phonons obtained from phonon dispersion relations for graphene and strong anharmonicity of Brenner-II potential resulting in high phonon–phonon scattering rates [50]. The long-range van der Waals interactions added to the Brenner-II potential in AIREBO may further increase the phonon scattering rate, thus additionally reducing the value of k. While the variability of the results of experimental measurements of thermal conductivity of individual CNTs [1–8] prevents a direct quantitative validation of interatomic potentials, the understanding of the degree to which the choice of interatomic potential can affect the predictions of the simulations may help in resolving some of the discrepancies in published MD results and may assist in design and interpretation of future computational studies. Moreover, despite the lack of quantitative predictive power of current MD calculations of thermal conductivity, the qualitative trends revealed in the simulations, such as the CNT length dependence shown in Fig. 3, are still consistent across studies undertaken with different interatomic potentials. These qualitative trends are certainly of interest for the design of CNT materials with thermal transport properties tailored for particular practical applications.

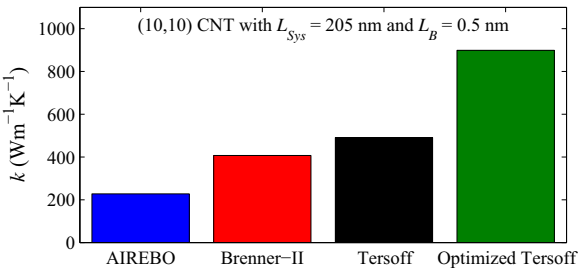

Fig. 8. Thermal conductivity, k, predicted in NEMD simulations performed with four different interatomic potentials for identical CNTs under identical computational conditions.

4. Summary

The results of a systematic investigation of the effect of various computational parameters on the values of thermal conductivity of CNTs predicted in MD simulations uncover some of the key reasons for the wide variability of the computational predictions reported in the literature and provide guidance for designing simulation setups that reduce the ambiguity in data interpretation.

The CNT length dependence of thermal conductivity is investigated in a broad range of nanotube lengths, from 47 nm to 630 nm, and is found to exhibit a gradual transition from a strong length dependence for CNTs shorter than ~200 nm to a much weaker dependence for longer CNTs. This dependence is characteristic of the transition from ballistic to diffusive-ballistic heat transport regimes and has been observed in many of the earlier studies. A detailed analysis of the CNT length dependence reveals that, in NEMD simulations with uni-directional heat flux implementation, the effect of increasing length of the central part of the nanotube, L_C, is nearly indistinguishable from the effect of increasing length of the heat bath regions, L_B. This observation suggests that the common practice of neglecting the length of the heat bath regions when defining the CNT length in NEMD simulations may introduce an uncertainty in interpretation of the results, as the variability of L_B in different studies may translate into a substantial variability in the predicted values of thermal conductivity. The results of this study suggest that the total length of a CNT (*including* the length of the heat bath regions) should be used as the definition of the CNT length in NEMD simulations with uni-directional heat flux. To provide an adequate representation of the true nature of the system being modeled, the length of the heat bath regions should be short relative to the overall CNT length. The length dependence of k in bi-directional flux implementations, commonly used with periodic boundary conditions, is also shown to be best represented by the definition of the effective CNT length comprised of the length of the heat bath regions and the length of an unperturbed part of the CNT between the hot and cold heat bath regions. This convention yields values of k that are consistent between the two (uni- and bi-directional) implementations of the heat flux in NEMD simulations.

The effect of the choice of the interatomic potential on the value of thermal conductivity predicted in NEMD simulations is also quantified in a series of simulations performed with several commonly used potentials. An up to a fourfold difference in the values of k is predicted with different potentials for identical CNTs and computational setups. This large difference suggests that quantitative agreement between the results obtained with different interatomic potentials should not be expected. Many of the qualitative trends revealed in the simulations, however, are consistent across studies employing different potentials and are providing useful insights into the mechanisms of the nanoscale thermal transport in CNTs. Overall, the results of the systematic evaluation of the effect of the boundary conditions, size and location of the heat bath regions, definition of the CNT length, and the choice of interatomic potential on the predictions of NEMD simulations clarify the origins of quantitative discrepancies across published data and provide recommendations on the choice of computational

parameters that may reduce some of the inconsistencies between the computational results.

Acknowledgements

Financial support of this work is provided by the National Science Foundation (Grant CBET-1033919) and the Air Force Office of Scientific Research (Award FA9550-10-10545). Computational support is provided by the Oak Ridge Leadership Computing Facility (Project MAT048) and the National Science Foundation through the Extreme Science and Engineering Discovery Environment (Projects TG-DMR130010 and TG-DMR110090).

References

[1] C. Yu, L. Shi, Z. Yao, D. Li, A. Majumdar, Thermal conductance and thermopower of an individual single-wall carbon nanotube, Nano Lett. 5 (2005) 1842–1846.
[2] M. Fujii, X. Zhang, H. Xie, H. Ago, K. Takahashi, T. Ikuta, H. Abe, T. Shimizu, Measuring the thermal conductivity of a single carbon nanotube, Phys. Rev. Lett. 95 (2005) 065502.
[3] H.-Y. Chiu, V.V. Deshpande, H.W.Ch. Postma, C.N. Lau, C. Miko, L. Forro, M. Bockrath, Ballistic phonon thermal transport in multiwalled carbon nanotubes, Phys. Rev. Lett. 95 (2005) 226101.
[4] E. Pop, D. Mann, Q. Wang, K. Goodson, H. Dai, Thermal conductance of an individual single-wall carbon nanotube above room temperature, Nano Lett. 6 (2006) 96–100.
[5] S. Wang, Z. Liang, B. Wang, C. Zhang, High-strength and multifunctional macroscopic fabric of single-walled carbon nanotubes, Adv. Mater. 19 (2007) 1257–1261.
[6] I.-K. Hsu, R. Kumar, A. Bushmaker, S.B. Cronin, M.T. Pettes, L. Shi, T. Brintlinger, M.S. Fuhrer, J. Cumings, Optical measurement of thermal transport in suspended carbon nanotubes, Appl. Phys. Lett. 92 (2008) 063119.
[7] M.T. Pettes, L. Shi, Thermal and structural characterizations of individual single-, double-, and multi-walled carbon nanotubes, Adv. Funct. Mater. 19 (2009) 3918–3925.
[8] Q. Li, C. Liu, X. Wang, S. Fan, Measuring the thermal conductivity of individual carbon nanotubes by the raman shift method, Nanotechnology 20 (2009) 145702.
[9] S. Berber, Y.-K. Kwon, D. Tomanek, Unusually high thermal conductivity of carbon nanotubes, Phys. Rev. Lett. 84 (2000) 4613–4616.
[10] J. Che, T. Cagin, W.A. Goddard III, Thermal conductivity of carbon nanotubes, Nanotechnology 11 (2000) 65–69.
[11] M.A. Osman, D. Srivastava, Temperature dependence of the thermal conductivity of single-wall carbon nanotubes, Nanotechnology 12 (2001) 21–24.
[12] S. Maruyama, A molecular dynamics simulation of heat conduction in finite length (SWNTs), Physica B 323 (2002) 193–195.
[13] S. Maruyama, A molecular dynamics simulation of heat conduction of a finite length single-walled carbon nanotube, Microscale Thermophys. Eng. 7 (2003) 41–50.
[14] C.W. Padgett, D.W. Brenner, Influence of chemisorption on the thermal conductivity of single-wall carbon nanotubes, Nano Lett. 4 (2004) 1051–1053.
[15] J.F. Moreland, J.B. Freund, G. Chen, The disparate thermal conductivity of carbon nanotubes and diamond nanowires studied by atomistic simulation, Microscale Thermophys. Eng. 8 (2004) 61–69.
[16] M. Grujicic, G. Cao, B. Gersten, Atomic-scale computations of the lattice contribution to thermal conductivity of single-walled carbon nanotubes, Mater. Sci. Eng. B107 (2004) 204–216.
[17] M. Grujicic, G. Cao, W.N. Roy, Computational analysis of the lattice contribution to thermal conductivity of single-walled carbon nanotubes, J. Mater. Sci. 40 (2005) 1943–1952.
[18] G. Zhang, B. Li, Thermal conductivity of nanotubes revisited: effects of chirality, isotope impurity, tube length, and temperature, J. Chem. Phys. 123 (2005) 114714.
[19] K. Zhang, H. Fan, M.M.F. Yuen, Molecular dynamics study on thermal performance of CNT-array-thermal interface material, in: International Symposium on Electronic Materials and Packaging, IEEE, Kowloon, China, 2006, pp. 1–4.
[20] K. Bi, Y. Chen, J. Yang, Y. Wang, M. Chen, Molecular dynamics simulation of thermal conductivity of single-wall carbon nanotubes, Phys. Lett. A 350 (2006) 150–153.
[21] J.R. Lukes, H. Zhong, Thermal conductivity of individual single-wall carbon nanotubes, J. Heat Transfer 129 (2007) 705–716.
[22] R.-Q. Pan, Z.-J. Xu, Z.-Y. Zhu, Length dependence of thermal conductivity of single-walled carbon nanotubes, Chin. Phys. Lett. 24 (2007) 1321–1323.
[23] J. Shiomi, S. Maruyama, Molecular dynamics of diffusive-ballistic heat conduction in single-walled carbon nanotubes, Jpn. J. Appl. Phys. 47 (2008) 2005–2009.
[24] M. Alaghemandi, E. Algaer, M.C. Bohm, F. Muller-Plathe, The thermal conductivity and thermal rectification of carbon nanotubes studied using reverse non-equilibrium molecular dynamics simulations, Nanotechnology 20 (2009) 115704.
[25] C. Ren, W. Zhang, Z. Xu, Z. Zhu, P. Huai, Thermal conductivity of single-walled carbon nanotubes under axial stress, J. Phys. Chem. C 114 (2010) 5786–5791.
[26] J.A. Thomas, R.M. Iutzi, A.J.H. McGaughey, Thermal conductivity and phonon transport in empty and water-filled carbon nanotubes, Phys. Rev. B 81 (2010) 045413.
[27] B. Qiu, Y. Wang, Q. Zhao, X. Ruan, The effects of diameter and chirality on the thermal transport in free-standing and supported carbon-nanotubes, Appl. Phys. Lett. 100 (2012) 233105.
[28] A. Cao, J. Qu, Size dependent thermal conductivity of single-walled carbon nanotubes, J. Appl. Phys. 112 (2012) 013503.
[29] A.N. Imtani, Thermal conductivity for single-walled carbon nanotubes from Einstein relation in molecular dynamics, J. Phys. Chem. Solids 74 (2013) 1599–1603.
[30] R.A. Shelly, K. Toprak, Y. Bayazitoglu, Nose–Hoover thermostat length effect on thermal conductivity of single wall carbon nanotubes, Int. J. Heat Mass Transfer 53 (2010) 5884–5887.
[31] M.C.H. Wu, J.-Y. Hsu, Thermal conductivity of carbon nanotubes with quantum correction via heat capacity, Nanotechnology 20 (2009) 145401.
[32] H. Zhong, J.R. Lukes, Thermal conductivity of single-wall carbon nanotubes, in: Proceedings of IMECE04, Electronic and Photonic Packaging, Electrical Systems Design and Photonics, and Nanotechnology, ASME, Anaheim, CA, 2004, pp. 65–73.
[33] D.-L. Feng, Y.-H. Feng, Y. Chen, W. Li, X.-X. Zhang, Effects of doping stone-wales and vacancy defects on thermal conductivity of single-wall carbon nanotubes, Chin. Phys. B. 22 (2013) 016501.
[34] A.N. Volkov, R.N. Salaway, L.V. Zhigilei, Atomistic simulations, mesoscopic modeling, and theoretical analysis of thermal conductivity of bundles composed of carbon nanotubes, J. Appl. Phys. 114 (2013) 104301.
[35] R.-Q. Pan, Diameter and temperature dependence of thermal conductivity of single-walled carbon nanotubes, Chin. Phys. Lett. 28 (2011) 066104.
[36] Z. Xu, M.J. Buehler, Strain controlled thermomutability of single-walled carbon nanotubes, Nanotechnology 20 (2009) 185701.
[37] N. Wei, L. Xu, H.-Q. Wang, J.-C. Zheng, Strain engineering of thermal conductivity in graphene sheets and nanoribbons: a demonstration of magic flexibility, Nanotechnology 22 (2011) 105705.
[38] F. Nishimura, T. Takahashi, K. Watanabe, T. Yamamoto, Bending robustness of thermal conductance of carbon nanotubes: nonequilibrium molecular dynamics simulation, Appl. Phys. Express 2 (2009) 035003.
[39] Z. Xu, M.J. Buehler, Hierarchical nanostructures are crucial to mitigate ultrasmall thermal point loads, Nano Lett. 9 (2009) 2065–2072.
[40] C. Lin, H. Wang, W. Yang, The thermomutability of single-walled carbon nanotubes by constrained mechanical folding, Nanotechnology 21 (2010) 365708.
[41] A.N. Volkov, T. Shiga, D. Nicholson, J. Shiomi, L.V. Zhigilei, Effect of bending buckling of carbon nanotubes on thermal conductivity of carbon nanotube materials, J. Appl. Phys. 111 (2012) 053501.
[42] J. Shiomi, Private communication, 2010.
[43] A.M. Marconnet, M.A. Panzer, K.E. Goodson, Thermal conduction phenomena in carbon nanotubes and related nanostructured materials, Rev. Mod. Phys. 85 (2013) 1295–1326.
[44] J. Tersoff, New empirical approach for the structure and energy of covalent systems, Phys. Rev. B 37 (1988) 6991–7000.
[45] J. Tersoff, Empirical interatomic potential for carbon, with applications to amorphous carbon, Phys. Rev. Lett. 61 (1988) 2879–2882.
[46] D.W. Brenner, Empirical potential for hydrocarbons for use in simulating the chemical vapor deposition of diamond films, Phys. Rev. B 42 (1990) 9458–9471.
[47] S.J. Stuart, A.B. Tutein, J.A. Harrison, A reactive potential for hydrocarbons with intermolecular interactions, J. Chem. Phys. 112 (2000) 6472–6486.
[48] D.W. Brenner, O.A. Shenderova, J.A. Harrison, S.J. Stuart, B. Ni, S.B. Sinnott, A second-generation reactive empirical bond order (rebo) potential energy expression for hydrocarbons, J. Phys.: Condens. Matter 14 (2002) 783–802.
[49] W. Zhang, Z. Zhu, F. Wang, T. Wang, L. Sun, Z. Wang, Chirality dependence of the thermal conductivity of carbon nanotubes, Nanotechnology 15 (2004) 936–939.
[50] L. Lindsay, D.A. Broido, Optimized tersoff and brenner empirical potential parameters for lattice dynamics and phonon thermal transport in carbon nanotubes and graphene, Phys. Rev. B 81 (2010) 205441.
[51] Y. Yamaguchi, S. Maruyama, A molecular dynamics simulation of the fullerene formation process, Chem. Phys. Lett. 286 (1998) 336–342.
[52] J. Zhang, M. Tanaka, T. Matsumoto, A simplified approach for heat conduction analysis of CNT-based nano-composites, Comput. Methods Appl. Mech. Eng. 193 (2004) 5597–5609.
[53] C. Ren, Z. Xu, W. Zhang, Y. Li, Z. Zhu, P. Huai, Theoretical study of heat conduction in carbon nanotube hetero-junctions, Phys. Lett. A 374 (2010) 1860–1865.
[54] T. Schneider, E. Stoll, Molecular-dynamics study of a three-dimensional one-component model for distortive phase transitions, Phys. Rev. B 17 (1978) 1302–1322.
[55] A.N. Volkov, L.V. Zhigilei, Heat conduction in carbon nanotube materials: strong effect of intrinsic thermal conductivity of carbon nanotubes, Appl. Phys. Lett. 101 (2012) 043113.
[56] S. Plimpton, Fast parallel algorithms for short-range molecular dynamics, J. Comput. Phys. 117 (1995) 1–19.

[57] H.-C. Cheng, C.-H. Wu, W.-H. Chen, Low-temperature thermal conductivity of short single-walled carbon nanotubes using a modified Nose–Hoover thermostat, Nanoscale Microscale Thermophys. Eng. 16 (2012) 242–259.
[58] A.V. Savin, B. Hu, Y.S. Kivshar, Thermal conductivity of single-walled carbon nanotubes, Phys. Rev. B 80 (2009) 195423.
[59] J. Wang, J.-S. Wang, Carbon nanotube thermal transport: ballistic to diffusive, Appl. Phys. Lett. 88 (2006) 111909.
[60] D. Donadio, G. Galli, Thermal conductivity of isolated and interacting carbon nanotubes: comparing results from molecular dynamics and the boltzmann transport equation, Phys. Rev. Lett. 99 (2007) 255502.
[61] N. Mingo, D.A. Broido, Length dependence of carbon nanotube thermal conductivity and the "problem of long waves", Nano Lett. 5 (2005) 1221–1225.
[62] N. Mingo, D.A. Broido, Carbon nanotube ballistic thermal conductance and its limits, Phys. Rev. Lett. 95 (2005) 096105.
[63] H.-Y. Cao, H. Xiang, X.-G. Gong, Unexpected large thermal rectification in asymmetric grain boundary of graphene, Solid State Commun. 152 (2012) 1807–1810.
[64] J.E. Turney, E.S. Landry, A.J.H. McGaughey, C.H. Amon, Predicting phonon properties and thermal conductivity from anharmonic lattice dynamics calculations and molecular dynamics simulations, Phys. Rev. B 79 (2009) 064301.
[65] D.P. Sellan, E.S. Landry, J.E. Turney, A.J.H. McGaughey, C.H. Amon, Size effects in molecular dynamics thermal conductivity predictions, Phys. Rev. B 81 (2010) 214305.
[66] Z. Yao, J.-S. Wang, B. Li, G.-R. Liu, Thermal conduction of carbon nanotubes using molecular dynamics, Phys. Rev. B 71 (2005) 085417.
[67] P.K. Schelling, S.R. Phillpot, P. Keblinski, Comparison of atomic-level simulation methods for computing thermal conductivity, Phys. Rev. B 65 (2002) 144306.
[68] T. Watanabe, S.B. Sinnott, J.S. Tulenko, R.W. Grimes, P.K. Schelling, S.R. Phillpot, Thermal transport properties of uranium dioxide by molecular dynamics simulations, J. Nucl. Mater. 375 (2008) 388–396.
[69] X. Ni, G. Zhang, B. Li, Thermal conductivity and thermal rectification in unzipped carbon nanotubes, J. Phys.: Condens. Matter 23 (2011) 215301.
[70] J.-W. Jiang, J. Chen, J.-S. Wang, B. Li, Edge states induce boundary temperature jump in molecular dynamics simulation of heat conduction, Phys. Rev. B 80 (2009) 052301.
[71] D.J. Evans, Homogenous NEMD algorithm for thermal conductivity – application of non-canonical linear response theory, Phys. Lett. A 91 (1982) 457–460.